Myo-inositol concentration in MR spectroscopy for differentiating high grade glioma from primary central nervous system lymphoma.

Nagashima, Hiroaki ; Sasayama, Takashi ; Tanaka, Kazuhiro ; Kyotani, Katsusuke ; Sato, Naoko ; Maeyama, Masahiro ; Kohta, Masaaki ; Sakata,…

(Citation)
Journal of neuro-oncology.,136(2):317-326

(Issue Date)
2018-01

(Resource Type)
journal article

(Version)
Accepted Manuscript

Title: Myo-inositol concentration in MR spectroscopy for differentiating high grade glioma from primary central nervous system lymphoma

Authors:

Hiroaki Nagashima[1], Takashi Sasayama[1*], Kazuhiro Tanaka[1], Katsusuke Kyotani[2], Naoko Sato[1], Masahiro Maeyama[1], Masaaki Kohta[1], Junichi Sakata[1], Yusuke Yamamoto[1], Kohkichi Hosoda[1], Tomoo Itoh[3], Ryohei Sasaki[4], and Eiji Kohmura[1]

Affiliations:

[1]Department of Neurosurgery; [2]Center for Radiology and Radiation Oncology; [3]Department of Diagnostic Pathology; [4]Division of Radiation Oncology; Kobe University Graduate School of Medicine and Kobe University Hospital, Kobe 650-0017, Japan

***Corresponding author:**

Takashi Sasayama

Tel: (+81) 78-382-5966, Fax: (+81) 78-382-5979

E-mail: takasasa@med.kobe-u.ac.jp

Abbreviation

Cr: creatine

FWHM: full width at half maximum

Gln: glutamine,

Glu: glutamate

HGG: high-grade glioma

IDH: isocitrate dehydrogenase

ISYNA1: inositol 3-phosphate synthase

Lip: lipid

mIns: myo-inositol

MRI: Magnetic resonance imaging

MRS: Magnetic resonance spectroscopy

NAA: N-acetylaspartate

NAAG: N-acetylaspartylglutamate

PCNSL: primary central nervous system lymphoma

SNR: signal-to-noise ratio

Abstract

Conventional imaging of gliomas is non-specific and has limited value in their diagnosis. In this study, we assessed whether 3-T MR spectroscopy (MRS) with LCModel software might be useful for discriminating glioma from other brain tumors, such as primary central nervous system lymphomas (PCNSLs) and metastatic tumors. A total of 104 cases of brain tumor (66 gliomas, 20 PCNSLs, 6 metastatic tumors, 12 other tumors) were preoperatively investigated with short echo time (35 ms) single-voxel 3-T MRS. LCModel software was used to evaluate differences in the absolute concentrations of choline, N-acetylaspartate, N-acetylaspartylglutamate, glutamate, glutamine, myo-inositol (mIns), and lipid. mIns levels were significantly increased in high-grade glioma compared with PCNSL ($p < 0.001$). In multivariate logistic regression analysis, mIns was the best marker for differentiating high-grade glioma from PCNSL ($p < 0.001$, odds ratio 1.791977, 95% confidence interval 1.196549–3.084036). Conventional MRS detection of mIns resulted in a high diagnostic accuracy (sensitivity, 64%; specificity, 90%; area under the receiver operator curve, 0.80) for high-grade glioma. The expression of inositol 3-phosphate synthase (ISYNA1) was significantly higher in gliomas than in PCNSLs ($p < 0.05$), suggesting that the increased level of mIns in glioma is due to high expression of ISYNA1, the rate-limiting enzyme in the mIns-producing pathway. In conclusion,

noninvasive analysis of mIns using single-voxel MRS may be useful in distinguishing gliomas from other brain tumors, particularly PCNSLs.

Keywords: myo-inositol, MR spectroscopy, primary central nervous system lymphoma, Glioma, Metabolomics

Introduction

Glioma, especially high-grade glioma (HGG), is one of the most common brain tumors in adults and has one of the worst outcomes [1]. It is usually diagnosed via histological examination because there are not only no diagnostic biomarkers in the cerebrospinal fluid and serum, but also no specific imaging findings. A typical feature of HGG on magnetic resonance imaging (MRI) is a ring-like enhancing ill-demarcated mass lesion with peritumoral edema. However, this feature is quite similar to that of other brain tumors, such as metastatic tumors and primary central nervous system lymphomas (PCNSLs).

The standard treatment for glioma is maximal safe gross surgical resection, followed by radiotherapy and/or chemotherapy [2]. Stereotactic biopsy is usually performed for PCNSLs to obtain the histological diagnosis because PCNSLs are highly sensitive to chemotherapy and radiotherapy and the impact of the extent of resection on survival is low [3]. Total resection with craniotomy is occasionally performed for metastatic brain tumors. However, preoperative diagnosis of metastatic brain tumors is frequently made via imaging findings of multiple tumors in the brain and a primary tumor in another organ, in combination with tumor markers such as CEA and CA19-9 in the serum and/or cerebrospinal fluid [4, 5]. PCNSL is uncommon, representing approximately 3%–5% of

primary brain tumors, although its incidence has increased recently [6]. Because gliomas and PCNSLs have similar imaging findings (Fig. 1A) but require different surgical approaches, the development of a noninvasive preoperative detection method for these tumors is of clinical interest.

Arterial spin labeling and the apparent diffusion coefficient, which evaluate tumor vascularity and cellularity, are useful for the differentiation of these tumors [7-10]. Intravoxel incoherent motion and (F-18)2-deoxy-2-fluoro-D-glucose (FDG-PET) also play important roles in differentiating glioblastoma and PCNSL [11]. Although advanced MRI techniques, such as amide proton transfer-weighted imaging [12], can differentiate these two tumors, these methods are not readily available on mainstream clinical scanners.

Magnetic resonance spectroscopy (MRS) is unique in that it can noninvasively predict tumor type by evaluating metabolic information (Fig. 1B). Recent seminal studies reported the utility of conventional MRS in differential diagnosis. These reports indicated that the lipid/creatine ratio, glutamate/creatine ratio, glutamate/glutamate + glutamine ratio, and choline/creatine ratio on short echo time (TE) MRS may be useful in differentiating glioblastoma and PCNSL [13, 14]. However, lipids are affected by necrosis and glutamate is decreased by the isocitrate dehydrogenase (IDH) 1 mutation in some gliomas. In addition, these reports did not evaluate the diagnostic performance of MRS.

These findings motivated us to evaluate other metabolites that could more precisely distinguish gliomas from other brain tumors, especially PCNSLs, and to determine whether MRS could help in glioma diagnosis.

Methods

Study design and study population

Subjects were 115 patients with an intracranial tumor or a suspected intracranial brain tumor who were treated at the Department of Neurosurgery, Kobe University Hospital, between August 2013 and August 2016. This study was approved by the ethics review boards of our institutions (approval numbers: #1497 for MRS; #1579 for use of tumor samples). Informed consent was obtained from all patients prior to their inclusion in this study.

All patients underwent preoperative MRI and MRS within 1 week prior to surgery. Samples were resected during surgery at the exact targets indicated by MRS using an intraoperative navigation system (Brain LAB^{TM}) and immediately frozen in liquid nitrogen for subsequent investigation. Histopathological classification and tissue grading were performed by a board-certified neuropathologist. The IDH gene status of all glioma cases was analyzed by immunohistochemistry for IDH R132H and DNA sequencing of

IDH1 and IDH2. The IDH gene status of all PSNSL cases was analyzed by immunohistochemistry.

Of the 115 patients enrolled, 77 with glioma, 20 with PCNSL, 6 with metastatic tumor, and 12 with other tumors had high-quality MRS data as assessed by the objective criteria defined below in the section “MRI and MRS”. However, 11 were excluded before analysis of the correlation between MRS results: 3 had a signal-to-noise ratio (SNR) < 5 (anaplastic astrocytoma, n = 1; glioblastoma, n = 2), 1 had a full width at half maximum (FWHM) of more than 0.065 ppm (oligodendroglioma, n = 1), and 7 had a necrotic lesion with an insufficient volume of solid component (glioblastoma, n = 7). Thus, we ultimately analyzed 104 intra-axial brain tumor patients with glioma (grade I, n = 4; grade II, n = 17; grade III, n = 15; grade IV, n = 30), PCNSL (diffuse large B cell lymphoma, n = 20), metastatic tumor (lung cancer, n = 3; rectal cancer, n = 2, stomach cancer, n = 1), and other tumors (central neurocytoma, n = 3; meningioma, n = 3; germ cell tumor, n = 3; gliosis, n = 3). As a control, voxels were also placed in the same anatomical location on the contralateral (non-tumor) side of the brain (glioma, n = 60; PCNSL, n = 20). Of the 66 glioma patients, 3 had pilocytic astrocytoma, 1 had subependymal giant cell astrocytoma, 10 had diffuse astrocytoma, 9 had anaplastic astrocytoma, 30 had glioblastoma, 6 had oligodendroglioma, 6 had anaplastic oligodendroglioma, and 1 had

oligoastrocytoma.

All of the PCNSL patients were diagnosed with diffuse large B cell lymphoma. Mean patient age was significantly lower for those with gliomas (age range, 17–85 years; mean age, 55 ± 16 years) compared with those with PCNSLs (age range, 46–86 years; mean age, 60 ± 12). Of the 66 glioma patients, 57 (86%) were newly diagnosed. All of the PCNSL patients were newly diagnosed. Patients' clinical characteristics are summarized in 2.

MRI and MRS

The MRS signal was acquired using a 3.0-T MRI/1H-MRS scanner (Achieva; Philips Medical Systems, Best, The Netherlands) [15]. An 8-channel head MRI coil was used for signal reception and a quadrature body MRI coil was used for transmission of the radiofrequency pulses. Following routine preoperative MR imaging, FLAIR and T2* images were taken to localize the corresponding target. Single-voxel localized MR spectra were acquired using a double-echo point-resolved spectroscopic sequence (PRESS) with chemical-shift selective water suppression. The MRS acquisition parameters were as follows: volume of interest, $1.5 \times 1.5 \times 1.5$ cm^3; repetition time/TE = 2000/35 ms; number of acquisitions, 128 averages; and 1,024 complex points for the

spectral data. Volumes of interest were localized to representative areas of the solid tumor, which were assessed by a board-certified radiologist (RS) or technician (KK). Regions of necrosis, hemorrhage, or peripheral edema were excluded from the corresponding region. The unsuppressed water signal was obtained using the abovementioned parameters.

The FWHM and SNR of the MR spectra were assessed. Spectra with an FWHM of N-acetylaspartate (NAA) > 0.065 ppm or a SNR < 5 were excluded using these objective criteria. MRS data were quantified with LCModel version 6.3 (Stephen Provencher, Oakville, Ontario, Canada) using a basis set, which was developed using MR experiment simulation software (GAMMA, Radiology, Duke University Medical Center, Durham, NC) and calibrated with an MRS phantom. The basis set contained 19 metabolites (Supplementary Table 1). The water-suppressed spectral data were examined between 0.6 and 4.0 ppm. The absolute metabolite concentrations (mM) were estimated using the unsuppressed water signal as a reference. Absolute concentrations of choline (Cho), N-acetylaspartate (NAA) + N-acetylaspartylglutamate (NAAG), glutamate (Glu), glutamine (Gln), creatine (Cr), myo-inositol (mIns), lipid (Lip), lactate (Lac), and other metabolites are reported in mM.

Metabolites were quantified with Cramer–Rao lower bounds (CRLBs). The CRLB values were calculated from the residual error and the Fisher matrix of the partial

derivatives of the concentrations. These CRLB values reflect the variance of the spectra fitting estimate but not its accuracy, and they indicate how close repeated measurements will be to the current measurement under similar experimental conditions. All metabolites were excluded when the CRLB was > 30%.

Histological diagnosis and IDH gene status of clinical specimens

Surgical specimens were analyzed by a board-certified neuropathologist at Kobe University Hospital. Histological diagnosis and grading of the tissue were performed according to the 2007 WHO guidelines. IDH1 R132H analysis was confirmed via immunohistochemistry and DNA sequencing [16]. Detailed protocols are found in the Supplementary Materials and Methods.

Real-time PCR analysis

We also conducted integrated analyses of clinical samples (48 glioma and 39 PCNSL tumor samples) to examine expressions of various metabolic enzymes in the gliomas and PCNSLs. RNA extraction and real-time PCR analysis were performed as previously described [17]. Quantitative real-time PCR using TaqMan® Gene Expression Assays was performed using an Applied Biosystems 7500 real-time PCR system. The 18S ribosomal

RNA was used as the endogenous control. All reactions were performed in triplicate. The quantitative mRNA expression data were analyzed using the ΔΔCt method. The following TaqMan® Gene Expression Assays were used: ISYNA1 (SMID: Hs01126940_gH), IMPA1 (SMID: Hs04188597_m1), SLC5A3 (SMID: Hs00272857_s1), and 18S (SMID: Hs99999901_s1).

Statistical analysis

The Mann–Whitney U-test and Steel–Dwass test were used to examine statistical differences. Statistical significance was considered significant at $p < 0.05$. A multivariate logistic regression model analysis was used to determine the best predictor of the differential diagnosis of glioma and PCNSL. To assess diagnostic accuracy, receiver operating characteristic (ROC) curve analysis was used. Area under the ROC curve (AUC) values for discrimination were calculated. All statistical analysis was performed using the JMP 11 package (SAS Institute Japan, Tokyo, Japan).

Results

Metabolite concentrations among tumors

Because metabolites were excluded when the CRLB was > 30%, we analyzed 6

metabolites, Cho, NAA + NAAG, Glu, Gln, mIns, and Lip. First, we compared the concentrations of these metabolites among gliomas and other tumors (metastatic tumors, PCNSLs, and others). Glu and Lip levels were significantly lower in gliomas than in the other tumors, while mIns levels were significantly higher in gliomas than in the other tumors (Mann–Whitney nonparametric U-test, $p < 0.01$, $p < 0.05$, $p < 0.001$, respectively; Fig. 2). Cho, NAA + NAAG, and Gln were not significantly different between the two groups. mIns levels were significantly higher in gliomas than in metastatic tumors or PCNSLs, but there were no differences between gliomas and the contralateral normal brain (Steel–Dwass test, $p < 0.01$, $p < 0.001$, respectively; Supplementary Fig 1B). In addition, Lip levels were significantly lower in gliomas than in metastatic tumors or PCNSLs (Supplementary Fig. 1A). However, there were no significant differences between metastatic tumors and PCNSLs (Supplementary Fig. 1A). There were no significant differences in mIns and Lip levels between gliomas and other tumors (Supplementary Fig. 1A). These results suggest that mIns, Glu, and Lip could be differential metabolites between glioma and other tumors.

Metabolite concentrations based on glioma grade

Next, to determine whether metabolites are affected by the glioma tumor grade, we

compared the concentrations of the 6 metabolites among grades I, II, III, and IV. Glu, Gln, and Lip concentrations showed a clear trend for an increase from grades II to IV (Steel–Dwass test, $p < 0.05$, $p < 0.001$; Fig. 3A). Cho, NAA + NAAG, and mIns concentrations were not significantly different among tumor grades. However, the mIns concentration in grade IV glioma (glioblastoma) tended to be decreased compared with other grades. The mIns/Cr ratio was not significantly different among glioma grades (Fig. 3B).

Due to the metabolic change caused by the IDH mutation, we investigated the levels of metabolites in gliomas according to the presence of IDH wild-type and IDH mutant. Twenty-three gliomas had IDH1 mutantation and 39 had wild-type IDH1. The Glu concentration was significantly lower in IDH mutant glioma than in IDH wild-type glioma (Mann-Whiteny U- test, $p < 0.001$; Supplementary Fig. 2). There were no significant differences in the concentrations of Glu, Gln, Lip, Cho, and NAA + NAAG between IDH mutant glioma and IDH wild-type glioma (Supplementary Fig. 2 and data not shown).

Myo-inositol is a useful differential metabolite between glioma and PCNSL

Because the MRI features are quite similar between HGG and PCNSL and because it is difficult to diagnose HGG and PCNSL, we investigated the metabolic changes in HGG

and PCNSL. Glu and Lip levels were significantly higher in PCNSLs than in HGGs (Mann–Whitney U-test, $p < 0.05$, $p < 0.001$, respectively; Fig. 4A). Gln and mIns levels were significantly lower in PCNSLs than in HGGs (Mann–Whitney U-test, $p < 0.01$, $p < 0.001$, respectively; Fig. 4A). There was no difference in mIns levels between metastatic brain tumor and PCNSLs (Supplementary Fig. 3). However, the mIns concentration was higher in HGG than in PCNSL and the mIns/Cr ratio was not significantly different between HGG and PCNSL. HGG had a slightly higher concentration of Cr ($p < 0.05$; Supplementary Fig. 4). In multivariate logistic regression analysis, mIns ($p < 0.001$; odds ratio [OR] 1.791977, 95% confidence interval [CI] 1.196549–3.084036) and Glu ($p < 0.05$, OR 0.0379, 95% CI 0.353138–0.974641) were significant variables that could be used to independently differentiate HGG from PCNSL (Table 1).

Next, we investigated the discriminatory power of mIns in HGG and other tumors using the ROC curve method. ROC curve analysis gave the following results: mIns concentration > 3.63 mM was 64% sensitive and 90% specific for differentiating HGG from PCNSL (AUC 0.80; Fig. 4B); but Glu concentration < 6.61 mM was 91% sensitive and 40% specific for differentiating HGG from PCNSL (AUC 0.68; data not shown). Using the respective mIns concentration of 3.63 mM and Glu concentration of 6.61 mM, the diagnostic sensitivity and specificity of the algorithm were improved to 69% and 95%,

respectively (AUC 0.85; Fig. 4B). Although combined evaluation of mIns and Glu had relatively high sensitivity and specificity compared with mIns alone, there was no difference between mIns + Glu and mIns alone for discriminating HGG. These results indicate that mIns may be the most useful metabolite for differentiating HGG from PCNSL in MRS. In addition, mIns concentration < 2.96 mM was 77% sensitive and 85% specific for differentiating HGG from PCNSL and metastatic tumor (AUC 0.85; Supplementary Fig. 5).

Because there are three metabolic enzymes in the mIns-producing pathway—ISYNA1 (inositol 3-phosphate synthase), IMPA1/2 (myo-inositol 3-phosphate monophosphatase), and SLC5A3 (solute carrier family 5/inositol transporter, member 3; Supplementary Fig. 6A)—we examined the mRNA expressions of these enzymes in the tumor tissues of gliomas and PCNSLs. The expression of ISYNA1, the rate-limiting enzyme that catalyzes the first step in the biosynthesis of mIns, was significantly higher in gliomas than in PCNSLs ($p < 0.001$; Fig. 4C), although there were no significant differences in IMPA1/2 and SLC5A3 levels. In particular, astrocytic gliomas had significantly higher expression of ISYNA1 than PCNSLs ($p < 0.001$; Supplementary Fig. 6B).

Discussion

This study shows that mIns, Glu, and Lip are useful diagnostic metabolites in gliomas. Furthermore, mIns and Glu are useful differential metabolites between HGG and PCNSLs. In particular, the levels of mIns were significantly higher in gliomas than in PCNSLs. Conventional MRS detection of mIns had a high diagnostic accuracy (AUC 0.80) for HGG.

mIns is one of the most abundant metabolites in the brain, with a peak at 3.56 ppm on short TE MRS. It is a sugar-like molecule that acts as an osmolyte and is involved in various key biochemical processes, such as signal transduction [18], phosphorylation of target proteins [19], chromatin remodeling and gene expression [20], and mRNA transport [21]. The brain manifests very high levels of mIns, particularly in astrocytes [22, 23]. The mIns concentration is increased in various brain disorders including reactive astrogliosis and brain tumors (ependymomas and choroid plexus papillomas). In the present study, the mIns concentration was not significantly different among glioma grades, in line with a previous report [24]. Some authors have shown that the mIns/Cr ratio is higher in low-grade astrocytoma than in HGG [23], but the mIns/Cr ratio in our study was not significantly different among glioma grades.

A previous study found that mIns was useful for discriminating PCNSL and astrocytomas on 1.5-T short TE MRS [12]. However, to the best of our knowledge, ours

is the first study to show the diagnostic accuracy of mIns in discriminating HGG and PCNSL using 3-T MRS with LCModel software. In addition, we found no difference in the mIns/Cr ratio between HGG and PCNSL, in line with previous studies [13, 14], because the Cr concentration was higher in HGG than in PCNSL [13]. Cr is widely known to be a marker of cellular energy and correlates with cell density and Cr has been used as an internal control. However, to distinguish HGG from PCNSL, concentration of the mIns seems to be more useful than mIns/Cr ratio.

We also analyzed the mRNA expression of metabolic enzymes related to mIns in tumor tissues. The expression level of ISYNA1 was found to be significantly increased in gliomas compared with PCNSLs. ISYNA1 is a rate-limiting enzyme that catalyzes the first step in the biosynthesis of mIns. It converts glucose-6-phosphate to inositol-1-phosphate, which is then dephosphorylated by IMPA1 to synthesize mIns [25]. Several studies have suggested the hormonal regulation of ISYNA1 expression, but very little is known about the regulation of ISYNA1. Seelan and coworkers [26] reported that E2F1, a transcription factor promoting the cell cycle, could upregulate ISYNA1 expression. Notably, Wei et al. [27] showed that a high concentration of mIns in tumors is associated with high levels of ISYNA1. In addition, because ISYNA1 is the rate-limiting enzyme in myo-inositol biosynthesis, myo-inositol biosynthesis is equivalent to myo-inositol 1-

phosphate biosynthesis [28]. In the present study, the mRNA levels of ISYNA1 were significantly elevated in glioma tissue compared with PCNSLs. These findings suggest that the expression levels of ISYNA1 may affect the mIns concentration in brain tumors. Glu was also a significant variable that could be used to independently differentiate HGG from PCNSL, in line with a previous report [13]. Interestingly, the Glu level was significantly lower in HGGs than PCNSLs, although the Gln level was significantly higher in HGGs than PCNSLs. Glu is one of the most abundant metabolites in the body. It acts as an excitatory neurotransmitter and is largely synthesized in neurons and glial cells. Extracellular Gln released from neurons is taken up by glutamine transporters in glial cells and rapidly converted to Glu by glutaminase. In glioma, glutamine transporter (SNAT3) is upregulated via the mTOR signaling pathway, one of the most important activated pathways in glioma [29]. Moreover, glutamate dehydrogenase, the enzyme that converts Glu to α-ketoglutarate in mitochondria, is upregulated in human glioma tissues [30]. We could not find any pertinent study regarding glutamine metabolism in PCNSL, but myc-driven lymphomas are dependent on glutamine uptake and metabolism and the glutaminase splice variant C is enriched in lymphoma [31]. Recent work showed that the IDH1 mutation alters Glu metabolism and leads to a lower Glu concentration [32]. However, the IDH1 mutation was usually identified in lower-grade gliomas (grade II–III),

not grade IV (glioblastoma) [33], and there were only two patients with IDH mutant grade IV glioma in this study. The Glu concentration was not different between IDH1 wild-type glioma and PCNSL, although it was significantly different between IDH1 mutant glioma and PCNSL (Supplementary Fig. 2). Therefore, further study is necessary to determine the role of Glu as a differential biomarker of glioma and PCNSL.

Lip, with a peak at 1.2 ppm, is a useful biomarker to discriminate between PCNSL and glioblastoma on short TE MRS [14, 34]. A recent study showed that total Lip levels tend to be higher in HGG than in glioma [36]. Therefore, a selection bias may have led to a low Lip concentration in the HGG group in this study. In addition, Lip seemed to be related to tumor necrosis, which is considered an indicator of malignancy and poor prognosis [35, 36]. Therefore, evaluation of Lip alone may be insufficient to discriminate HGG and PCNSL.

There are some limitations to this study. First, the study was retrospective and the sample size was small. In particular, there were few metastatic and other tumors. A prospective large-scale validation study is thus needed. Second, we excluded 11 glioma patients due to a low SNR, high FWHM, or necrosis, which might represent a selection bias. Third, the mIns peak overlaps with the glycine peak and unambiguous assignment of the glycine signal may not be possible, especially at a short TE. Indeed, a high glycine

level has been found in glioblastomas [37]. Because glycine is detectable at a long TE, we have to use additional long TE manual data to distinguish the glycine peak from mIns. Otherwise, ex vivo analysis of the concentrations of mIns and glycine in tumor tissues using mass spectrometry is needed. Finally, although the precision of the cutoff values for maximal diagnostic accuracy were set in this study, some myoinositol value overlaps in HGG and PCNSL. However, mIns may be incorporated within diagnostic algorithms in clinical practice to discriminate HGG from PCNSLs.

In conclusion, mIns levels may be a useful diagnostic marker for gliomas. MRS evaluation of mIns could provide quantitative information for differentiating HGG from PCNSL. MRS may be useful as an adjunct to another modality for the diagnosis of HGG and PCNSL.

Acknowledgments

We appreciate those at the Brain Tumor Translational Resource at Kobe University for access to biospecimens and for biorepository support.

References

1. Stupp R, Pavlidis N, Jelic S (2005) ESMO Minimum Clinical Recommendations for diagnosis, treatment and follow-up of malignant glioma. Annals of oncology: official journal of the European Society for Medical Oncology 16 Suppl 1: i64-65 doi:10.1093/annonc/mdi834

2. Stupp R (2007) Malignant glioma: ESMO clinical recommendations for diagnosis, treatment and follow-up. Annals of oncology: official journal of the European Society for Medical Oncology 18 Suppl 2: ii69-70 doi:10.1093/annonc/mdm044

3. Morris PG, Abrey LE (2009) Therapeutic challenges in primary CNS lymphoma. The Lancet Neurology 8: 581-592 doi: 10.1016/s1474-4422(09)70091-2

4. Arrieta O, Saavedra-Perez D, Kuri R, Aviles-Salas A, Martinez L, Mendoza-Posada D, Castillo P, Astorga A, Guzman E, De la Garza J (2009) Brain metastasis development and poor survival associated with carcinoembryonic antigen (CEA) level in advanced non-small cell lung cancer: a prospective analysis. BMC cancer 9: 119 doi: 10.1186/1471-2407-9-119

5. Christensen TD, Spindler KL, Palshof JA, Nielsen DL (2016) Systematic review: brain metastases from colorectal cancer--Incidence and patient characteristics. BMC cancer 16: 260 doi: 10.1186/s12885-016-2290-5

6. Haldorsen IS, Krossnes BK, Aarseth JH, Scheie D, Johannesen TB, Mella O, Espeland A (2007) Increasing incidence and continued dismal outcome of primary central nervous system lymphoma in Norway 1989-2003 : time trends in a 15-year national survey. Cancer 110: 1803-1814 doi:10.1002/cncr.22989

7. Guo AC, MacFall JR, Provenzale JM (2002) Multiple sclerosis: diffusion tensor MR imaging for evaluation of normal-appearing white matter. Radiology 222: 729-736 doi:10.1148/radiol.2223010311

8. Weber MA, Zoubaa S, Schlieter M, Juttler E, Huttner HB, Geletneky K, Ittrich C, Lichy MP, Kroll A, Debus J, Giesel FL, Hartmann M, Essig M (2006) Diagnostic performance of spectroscopic and perfusion MRI for distinction of brain tumors. Neurology 66: 1899-1906 doi:10.1212/01.wnl.0000219767.49705.9c

9. Yamasaki F, Kurisu K, Satoh K, Arita K, Sugiyama K, Ohtaki M, Takaba J, Tominaga A, Hanaya R, Yoshioka H, Hama S, Ito Y, Kajiwara Y, Yahara K, Saito T, Thohar MA (2005) Apparent diffusion coefficient of human brain tumors at MR imaging. Radiology 235: 985-991 doi:10.1148/radiol.2353031338

10. Le Bihan D, Breton E, Lallemand D, Grenier P, Cabanis E, Laval-Jeantet M (1986) MR imaging of intravoxel incoherent motions: application to diffusion and perfusion in neurologic disorders. Radiology 161: 401-407

doi:10.1148/radiology.161.2.3763909

11. Yamashita K, Hiwatashi A, Togao O, Kikuchi K, Kitamura Y, Mizoguchi M, Yoshimoto K, Kuga D, Suzuki SO, Baba S, Isoda T, Iwaki T, Iihara K, Honda H (2016) Diagnostic utility of intravoxel incoherent motion mr imaging in differentiating primary central nervous system lymphoma from glioblastoma multiforme. Journal of magnetic resonance imaging: JMRI 44: 1256-1261 doi:10.1002/jmri.25261

12. Jiang S, Yu H, Wang X, Lu S, Li Y, Feng L, Zhang Y, Heo HY, Lee DH, Zhou J, Wen Z (2016) Molecular MRI differentiation between primary central nervous system lymphomas and high-grade gliomas using endogenous protein-based amide proton transfer MR imaging at 3 Tesla. European radiology 26: 64-71 doi: 10.1007/s00330-015-3805-1

13. Aburano H, Ueda F, Yoshie Y, Matsui O, Nakada M, Hayashi Y, Gabata T (2015) Differences between glioblastomas and primary central nervous system lymphomas in 1H-magnetic resonance spectroscopy. Japanese journal of radiology 33: 392-403 doi: 10.1007/s11604-015-0430-5

14. Yamasaki F, Takayasu T, Nosaka R, Amatya VJ, Doskaliyev A, Akiyama Y, Tominaga A, Takeshima Y, Sugiyama K, Kurisu K (2015) Magnetic resonance spectroscopy detection of high lipid levels in intraaxial tumors without central necrosis:

a characteristic of malignant lymphoma. Journal of neurosurgery 122: 1370-1379 doi:10.3171/2014.9.jns14106

15. Provencher SW (2001) Automatic quantitation of localized in vivo 1H spectra with LCModel. NMR in biomedicine 14: 260-264

16. Tanaka K, Sasayama T, Mizukawa K, Takata K, Sulaiman NS, Nishihara M, Kohta M, Sasaki R, Hirose T, Itoh T, Kohmura E (2015) Combined IDH1 mutation and MGMT methylation status on long-term survival of patients with cerebral low-grade glioma. Clinical neurology and neurosurgery 138: 37-44 doi:10.1016/j.clineuro.2015.07.019

17. Tanaka K, Sasayama T, Irino Y, Takata K, Nagashima H, Satoh N, Kyotani K, Mizowaki T, Imahori T, Ejima Y, Masui K, Gini B, Yang H, Hosoda K, Sasaki R, Mischel PS, Kohmura E (2015) Compensatory glutamine metabolism promotes glioblastoma resistance to mTOR inhibitor treatment. The Journal of clinical investigation 125: 1591-1602 doi: 10.1172/jci78239

18. Berridge MJ, Lipp P, Bootman MD (2000) Signal transduction. The calcium entry pas de deux. Science 287: 1604-1605

19. Saiardi A, Bhandari R, Resnick AC, Snowman AM, Snyder SH (2004) Phosphorylation of proteins by inositol pyrophosphates. Science 306: 2101-2105

doi:10.1126/science.1103344

20. Shen X, Xiao H, Ranallo R, Wu WH, Wu C (2003) Modulation of ATP-dependent chromatin-remodeling complexes by inositol polyphosphates. Science 299: 112-114 doi:10.1126/science.1078068

21. York JD, Odom AR, Murphy R, Ives EB, Wente SR (1999) A phospholipase C-dependent inositol polyphosphate kinase pathway required for efficient messenger RNA export. Science 285: 96-100

22. Haris M, Cai K, Singh A, Hariharan H, Reddy R (2011) In vivo mapping of brain myo-inositol. NeuroImage 54: 2079-2085 doi:10.1016/j.neuroimage.2010.10.017

23. Castillo M, Smith JK, Kwock L (2000) Correlation of myo-inositol levels and grading of cerebral astrocytomas. AJNR American journal of neuroradiology 21: 1645-1649

24. Hattingen E, Raab P, Franz K, Zanella FE, Lanfermann H, Pilatus U (2008) Myo-inositol: a marker of reactive astrogliosis in glial tumors? NMR in biomedicine 21: 233-241 doi:10.1002/nbm.1186

25. Koguchi T, Tanikawa C, Mori J, Kojima Y, Matsuda K (2016) Regulation of myo-inositol biosynthesis by p53-ISYNA1 pathway. International journal of oncology 48: 2415-2424 doi:10.3892/ijo.2016.3456

26. Seelan RS, Lakshmanan J, Casanova MF, Parthasarathy RN (2009) Identification of myo-inositol-3-phosphate synthase isoforms: characterization, expression, and putative role of a 16-kDa gamma(c) isoform. The Journal of biological chemistry 284: 9443-9457 doi:10.1074/jbc.M900206200

27. Wei L, Hong S, Yoon Y, Hwang SN, Park JC, Zhang Z, Olson JJ, Hu XP, Shim H (2012) Early prediction of response to Vorinostat in an orthotopic rat glioma model. NMR in biomedicine 25: 1104-1111 doi:10.1002/nbm.2776

28. Eisenberg F Jr, Parthasarathy R (1987) Measurement of biosynthesis of myo-inositol from glucose 6-phosphate. Methods Enzymol 141: 127-43

29. Sidoryk M, Matyja E, Dybel A, Zielinska M, Bogucki J, Jaskolski DJ, Liberski PP, Kowalczyk P, Albrecht J (2004) Increased expression of a glutamine transporter SNAT3 is a marker of malignant gliomas. Neuroreport 15: 575-578

30. Zhang J, Wang G, Mao Q, Li S, Xiong W, Lin Y, Ge J (2016) Glutamate dehydrogenase (GDH) regulates bioenergetics and redox homeostasis in human glioma. Oncotarget doi:10.18632/oncotarget.7657

31. Gao P, Tchernyshyov I, Chang TC, Lee YS, Kita K, Ochi T, Zeller KI, De Marzo AM, Van Eyk JE, Mendell JT, Dang CV (2009) c-Myc suppression of miR-23a/b enhances mitochondrial glutaminase expression and glutamine metabolism. Nature 458:

762-765 doi: 10.1038/nature07823

32. Nagashima H, Tanaka K, Sasayama T, Irino Y, Sato N, Takeuchi Y, Kyotani K, Mukasa A, Mizukawa K, Sakata J, Yamamoto Y, Hosoda K, Itoh T, Sasaki R, Kohmura E (2016) Diagnostic value of glutamate with 2-hydroxyglutarate in magnetic resonance spectroscopy for IDH1 mutant glioma. Neuro-oncology 18: 1559-1568 doi:10.1093/neuonc/now090

33. Parsons DW, Jones S, Zhang X, Lin JC, Leary RJ, Angenendt P, Mankoo P, Carter H, Siu IM, Gallia GL, Olivi A, McLendon R, Rasheed BA, Keir S, Nikolskaya T, Nikolsky Y, Busam DA, Tekleab H, Diaz LA, Jr., Hartigan J, Smith DR, Strausberg RL, Marie SK, Shinjo SM, Yan H, Riggins GJ, Bigner DD, Karchin R, Papadopoulos N, Parmigiani G, Vogelstein B, Velculescu VE, Kinzler KW (2008) An integrated genomic analysis of human glioblastoma multiforme. Science 321: 1807-1812 doi:10.1126/science.1164382

34. Mora P, Majos C, Castaner S, Sanchez JJ, Gabarros A, Muntane A, Aguilera C, Arus C (2014) (1)H-MRS is useful to reinforce the suspicion of primary central nervous system lymphoma prior to surgery. European radiology 24: 2895-2905 doi: 10.1007/s00330-014-3308-5

35. Kimura T, Sako K, Gotoh T, Tanaka K, Tanaka T (2001) In vivo single-voxel

proton MR spectroscopy in brain lesions with ring-like enhancement. NMR in biomedicine 14: 339-349

36. Opstad KS, Ladroue C, Bell BA, Griffiths JR, Howe FA (2007) Linear discriminant analysis of brain tumour (1)H MR spectra: a comparison of classification using whole spectra versus metabolite quantification: NMR Biomed 20: 763-770 doi: 10.1002/nbm.1147

37. Choi C, Ganji SK, DeBerardinis RJ, Dimitrov IE, Pascual JM, Bachoo R, Mickey BE, Malloy CR, Maher EA (2011) Measurement of glycine in the human brain in vivo by 1H-MRS at 3 T: application in brain tumors. Magnetic resonance in medicine 66: 609-618 doi:10.1002/mrm.22857

Compliance with Ethical Standards

Disclosure of potential conflicts of interest: None

Research involving Human Participants and/or Animals: This study was approved by the ethics review boards of our institutions (approval numbers: #1497 for MRS; #1579 for use of tumor samples).

Informed consent: Informed consent was obtained from all patients prior to their inclusion in this study.

Funding: K. Tanaka is supported by grants from the Japanese Ministry of Education, Culture, Sports, Science and Technology (26462181), Takeda Science Foundation and Mochida Memorial Foundation for Medical and Pharmaceutical Research. T. Sasayama, K. Hosoda and E. Kohmura are supported by grants from the Japanese Ministry of Education, Culture, Sports, Science and Technology (25462258, 15K10302 and 25293309, respectively).

Conflict of Interest: The authors declare that they have no conflict of interest.

Figure legends

Figure 1

A. Upper panel: Glioblastoma (GBM) in a 39-year-old woman. Axial contrast- enhanced T1 weighted image (left) shows diffuse tumor enhancement in the left temporal lobe. Voxel (1.5×1.5×1.5cm) is located at left temporal lobe tumor. Apparent diffusion coefficient (ADC) shows low intensity in tumor (center). Diffusion weighted image (DWI) shows high intensity in tumor (right).

   Lower panel: Primary central nervous system lymphoma (PCNSL) in a 74-year-old man. Axial contrast- enhanced T1 weighted image (left) shows diffuse tumor enhancement in the left temporal lobe. Voxel (1.5×1.5×1.5cm) is located at left temporal lobe tumor. ADC shows low intensity in tumor (center). DWI shows high intensity in tumor (right).

B. Spectra image of single-voxel magnetic resonance spectroscopy (TE 35msec) in GBM and PCNSL (Figure 1A). Glu, glutamate; Gln, glutamine; NAA, N-acetylasparate; NAAG, N-acetylaspartylglutamate; Cho, choline; Cr, creatine; mIns, myo-Inositol; Lac, lactate; Lip, lipid.

Figure 2

Metabolic profiling of tumor samples assessed via in vivo MRS. Comparisons of the amount of metabolites in glioma, n = 66 and others, n = 38 (metastasis, n = 6; PCNSL, n = 20; other tumor, n = 12). The line shows the median. Box and whisker plots show the concentration range of metabolites; the box spans the 25th and 75th percentiles of the median; the whiskers represent the 0th and 100th percentiles. P values were calculated using Mann–Whitney nonparametric U test (*P < 0.05, ** P < 0.01, *** P < 0.001). Cho, choline; Glu, glutamate; Gln, glutamine; NAA, N-acetylasparate; NAAG, N-acetylaspartylglutamate; mIns, myo-Inositol; Lip, lipid; meta, metastatic tumor; PCNSL, primary central nervous system lymphoma.

Figure 3

A. Metabolic profiling of tumor samples assessed via in vivo MRS. Comparisons of the amount of metabolites in 66 glioma (grade I, n = 4; grade II, n = 17; grade III, n = 15; grade IV, n = 30).

B. Comparisons of Myo-inositol / Creatine ratio in 66 glioma. Box and whisker plots show the concentration range of metabolites; The line shows the median. The box spans the 25th and 75th percentiles of the median; the whiskers represent the 0th and 100th percentiles. P values were calculated using the Steel-Dwass test (*P < 0.05, **

P < 0.01, *** P < 0.001). Cho, choline; Glu, glutamate; Gln, glutamine; NAA, N-acetylasparate; NAAG, N-acetylaspartylglutamate; mIns, myo-Inositol; Lip, lipid.

Figure 4

A. Metabolic profiling of tumor samples assessed via in vivo MRS. Comparisons of the amount of metabolites in 45 high grade glioma (grade III, n = 15; grade IV, n = 30) and 20 primary central nervous system lymphoma. Box and whisker plots show the concentration range of metabolites; The line shows the median. The box spans the 25th and 75th percentiles of the median; the whiskers represent the 0th and 100th percentiles. P values were calculated using the Mann–Whitney nonparametric U test (*P < 0.05, ** P < 0.01, *** P < 0.001). Cho, choline; Glu, glutamate; Gln, glutamine; NAA, N-acetylasparate; NAAG, N-acetylaspartylglutamate; mIns, myo-Inositol; Lip, lipid. HGG, high grade glioma; PCNSL, primary central nervous system lymphoma.
B. ROC curve of the combination of myo-inositol and glutamate (blue line) and myo-inositol alone (red line) in differentiating high grade glioma from primary central nervous system lymphoma.
C. mRNA expression in of clinical samples (48 glioma and 39 PCNSL tumor samples) normalized to expression in normal brain. The line indicates the median. P values

were calculated using the Mann–Whitney nonparametric U test (**P<0.01, ***P< 0.001).

Table

Multivariate analysis of metabolites on differentiating HGG and PCNSL

Metabolite	p Value	OR	95% CI
NAA	0.139	0.60632	0.283726 – 1.16968
Cho	0.7498	1.129439	0.528887 – 2.478081
Glu	0.0379*	0.615811	0.353138 – 0.974641
Gln	0.1256	1.392545	0.913427 – 2.251243
mIns	0.0026***	1.791977	1.196549 – 3.084036
Lip	0.7068	0.995519	0.972845 – 1.020553

OR, odds ratio; CI, confidence interval; Cho, choline; Glu, glutamate; Gln, glutamine; NAA, N-acetylasparate; NAAG, N-acetylaspartylglutamate; mIns, myo-Inositol; Lip, lipid;

HGG, high grade glioma; PCNSL, primary central nervous system lymphoma

List of Supplementary Materials:

Supplementary detailed material and methods

Supplementary Figures

Supplementary Tables

Supplementary Detailed Material and Methods

***IDH* mutation analysis**

IDH1 R132H analysis was confirmed via immunohistochemistry and DNA sequencing. Paraffin sections of the intracranial tumor specimens were stained with *IDH1* R132H mutation-specific antibodies (1:50; H09 clone, Dianova). Genomic DNA was isolated from frozen glioma tissue using the DNeasy FFPE kit (QIAGEN) according to the manufacturer's instructions. To identify the *IDH* mutations, forward and reverse primers were designed that amplified exon 4 (codon R132) of the *IDH1* gene and exon 4 (codon R172) of the *IDH2* gene. Polymerase chain reaction (PCR) was performed using the following primers for *IDH1* R132: sense, 5'-TGAGAAGAGGGTTGAGGAGTTCAAGT-3'; antisense, 5'-AATGTGTTGAGATGGACGCCTATTTGT-3'; for *IDH2* R172: sense, 5'-AGCCCATCATCTGCAAAAAC-3'; antisense, 5'-CTAGGCGAGGAGCTCCAGT-3'.

The primers and the MinElute PCR Purification Kit (QIAGEN) were used to purify the PCR products. The DNA sequence was then analyzed and the presence/absence of mutations was assessed using Applied Biosystems DNA sequencers (Applied Biosystems) in the hotspot codons R132 in *IDH1* and R140 and R172 in *IDH2*.

Supplementary Figures

Supplementary Figure 1 (related to Figure 2)

A. Metabolic profiling of tumor samples assessed via in vivo MRS. Comparisons of the amount of metabolites in 104 brain tumor (glioma, n = 66; metastasis, n = 6; PCNSL, n = 20; other tumor, n = 12). The line shows the median. Box and whisker plots show the concentration range of metabolites; the box spans the 25th and 75th percentiles of the median; the whiskers represent the 0th and 100th percentiles. P values were calculated using the Steel-Dwass test (*P < 0.05, ** P < 0.01, *** P < 0.001). Cho, choline; Glu, glutamate; Gln, glutamine; NAA, N-acetylasparate; NAAG, N-acetylaspartylglutamate; mIns, myo-Inositol; Lip, lipid; meta, metastatic tumor; PCNSL, primary central nervous system lymphoma.

B. Myo-inositol in 92 intra-axial tumor glioma (glioma, n = 66; metastatic tumor, n = 6; primary central nervous system lymphoma, n = 20) and 80 contralateral normal brain. Box and whisker plots show the concentration range of metabolites; The line shows the median. The box spans the 25th and 75th percentiles of the median; the whiskers represent the 0th and 100th percentiles. P values were calculated using Steel-Dwass test (*P < 0.05, ** P < 0.01, *** P < 0.001). Cho, choline; Glu, glutamate; Gln, glutamine; NAA, N-acetylasparate; NAAG, N-

acetylaspartylglutamate; mIns, myo-Inositol; Lip, lipid. HGG, high grade glioma; PCNSL, primary central nervous system lymphoma.

Supplementary Figure 2 (related to Figure 3)

Metabolites concentration in 62 glioma (IDH1 mutant, n = 23; IDH1 wild, n = 39). Box and whisker plots show the concentration range of metabolites; The line shows the median. The box spans the 25th and 75th percentiles of the median; the whiskers represent the 0th and 100th percentiles. P values were calculated using Mann–Whitney nonparametric U test (*** $P < 0.001$).

Glu, glutamate; mIns, myo-Inositol;

Supplementary Figure 3 (related to Figure 3)

Myo-inositol in 71 intra-axial tumor glioma (high grade glioma, n = 45; metastatic tumor, n = 6; primary central nervous system lymphoma, n = 20). Box and whisker plots show the concentration range of metabolites; The line shows the median. The box spans the 25th and 75th percentiles of the median; the whiskers represent the 0th and 100th percentiles. P values were calculated using Steel-Dwass test (*$P < 0.05$, ** $P < 0.01$, *** $P < 0.001$). Cho, choline; Glu, glutamate; Gln, glutamine; NAA, N-acetylasparate; NAAG, N-acetylaspartylglutamate; mIns, myo-Inositol; Lip, lipid. HGG, high grade glioma; PCNSL, primary central nervous system lymphoma.

Supplementary Figure 4 (related to Figure 4)

Comparisons of Myo-inositol / Creatine ratio (left) and Creatine concentration (right) in 65 intra-axial tumor glioma (high grade glioma, n = 45; primary central nervous system lymphoma, n = 20). Box and whisker plots show the /Creatine ratio and concentration range of metabolites; The line shows the median. The box spans the 25th and 75th percentiles of the median; the whiskers represent the 0th and 100th percentiles. P values were calculated using the Mann–Whitney nonparametric U test (*P < 0.05, ** P < 0.01, *** P < 0.001). mIns, myo-Inositol; Cr , Creatine

Supplementary Figure 5 (related to Figure 4)

Receiver-operating characteristics (ROC) curve of the myo-inositol in differentiating high grade glioma from primary central nervous system lymphoma and metastatic tumor. HGG, high grade glioma; PCNSL, primary central nervous system lymphoma; meta, metastatic tumor; AUC, area under the ROC curve.

Supplementary Figure 6 (related to Figure 4)

A. Schematic showing the enzymes, transporters and metabolites related to myo-inositol. ISYNA1, inositol 3-phosphate synthase; IMPA1/2, myo-inositol 3-phosphate monophosphatase; SLC5A3, solute carrier family 5/ inositol transporter, member 3

B. mRNA expression in of clinical samples (36 astrocytic tumor, 11 oligodendroglial tumor and 39 PCNSL tumor samples) normalized to expression in normal brain. The line indicates the median. P values were calculated using the Mann–Whitney nonparametric U test (**P<0.01, ***P< 0.001). Oligo, oligodendroglioma + anaplastic oligodendroglioma; Astro, Diffuse astrocytoma + anaplastic astrocytoma + glioblastoma

Supplementary Table 1 List of measurable 19 metabolites in LC-Model

No.	Abbreviation	Metabolite
1	Ala	L-Alanine
2	Asp	Asparate
3	Cho	Choline
4	Cr	Creatine
5	GABA	Gamma-aminobutyric acid
6	Glc	Glucose
7	Gln	Glutamine
8	Glu	Glutamate
9	GPC	Glycerophosphocholine
10	GSH	Glutathione
11	PCh	Phosphocholine
12	PCr	Phosphocreatine
13	mIns	Myo-Inositol
14	Lac	Lactate
15	NAA	N-Acetylasparate
16	NAAG	N-Acetylaspartylglutamate
17	Scyllo	Scyllo-Inositol
18	-CrCH2	Creatine methylene group
19	2HG	2-hydroxyglutarate

Supplementary Table 2 Patient characteristics

		Glioma	PCNSL	Metastatic tumor	Other tumors
Number		66	20	6	12
Sex	M	38	11	2	7
	F	24	9	4	5
Mean Age ± SD		55±16	60±12	64±4	45±11
Pathology	PA	3			
	SEGA	1			
	DA	10			
	AA	9			
	GBM	30			
	OG	6			
	AOG	6			
	OA	1			
	DLBCL		20		
	Lung cancer			3	
	Rectal cancer			2	
	Stomach cancer			1	
	meningioma				3
	Germ cell tumor				3
	Central neurocytoma				3
	gliosis				3
WHO Grade	I	4			3
	II	17			6
	III	15			
	IV	30	20	6	
IDH1 mutation		23	0		
Newly diagnosed		57	20	6	12
Recurrence		9	0	0	0

DA: Diffuse Astrocytoma, AA: Anaplastic Astrocytoma

GBM: Glioblastoma, OG: Oligodendroglioma

AOG: Anaplastic OG, OA: Oligoastrocytoma
DLBCL: Diffuse Large B cell Lymphoma
PA; Pilocystic astrocytoma
SEGA; Subependymal giant cell astrocytoma

Figure 1

A

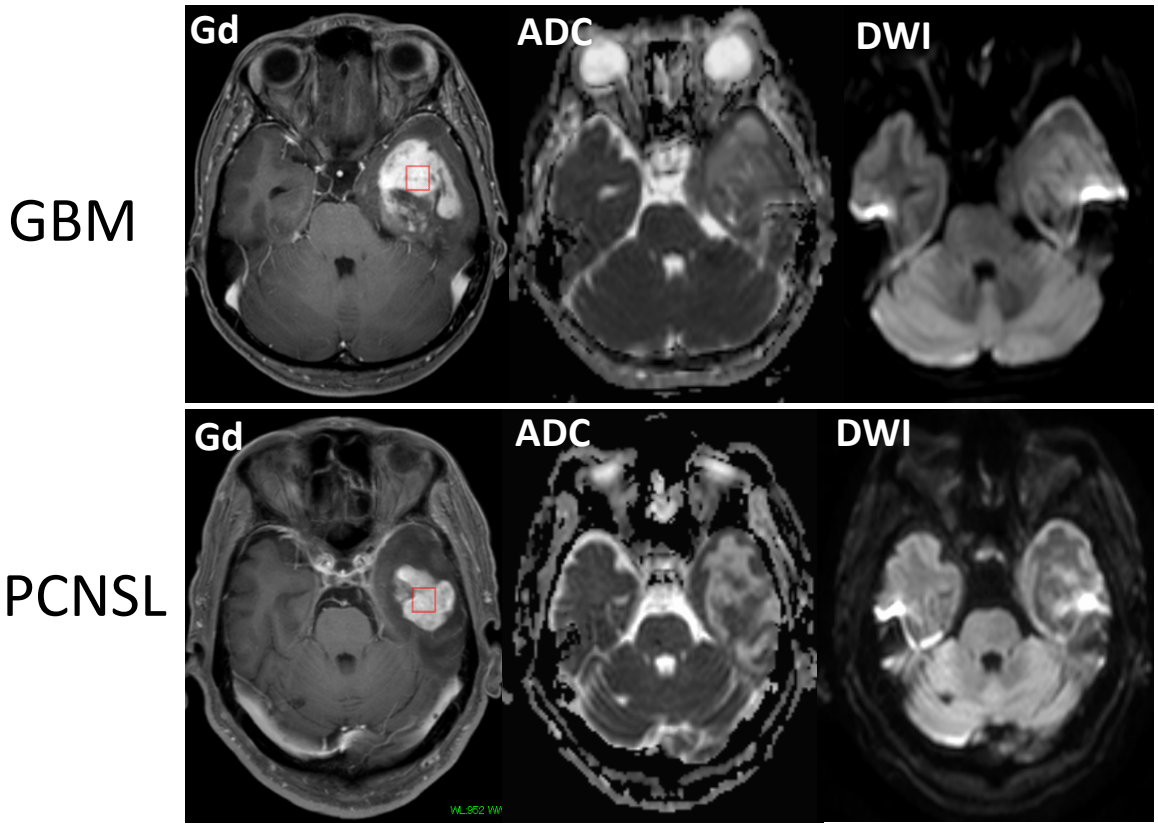
GBM
Gd
ADC
DWI
PCNSL
Gd
ADC
DWI

B

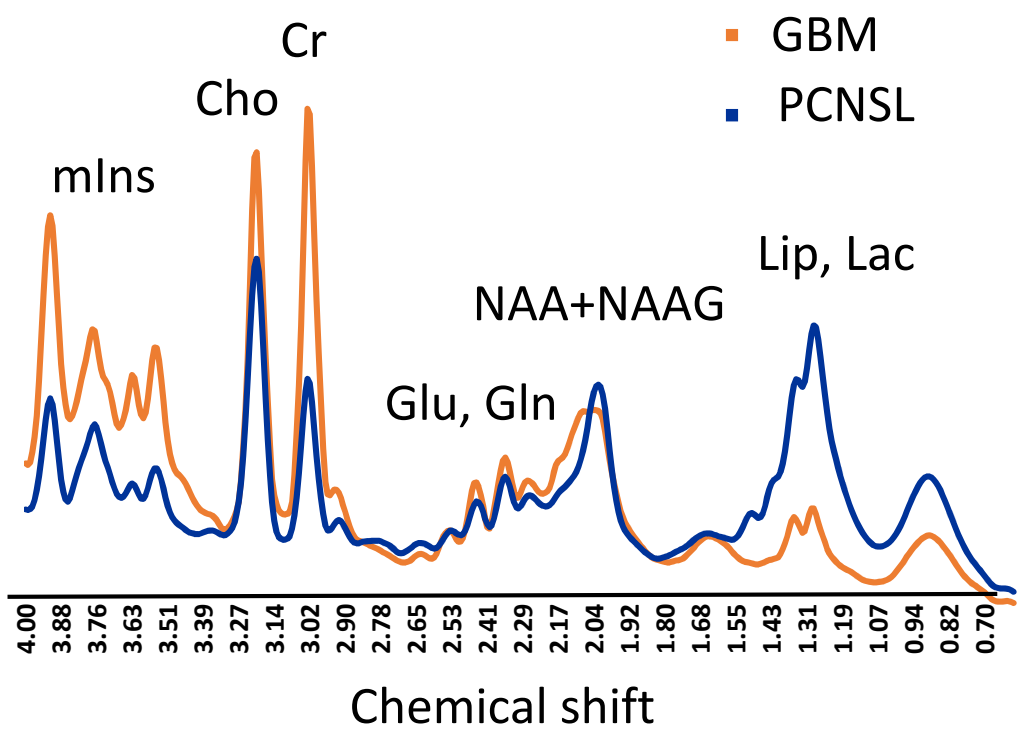
GBM
PCNSL
Cr
Cho
mIns
Lip, Lac
NAA+NAAG
Glu, Gln
4.00
3.88
3.76
3.63
3.51
3.39
3.27
3.14
3.02
2.90
2.78
2.65
2.53
2.41
2.29
2.17
2.04
1.92
1.80
1.68
1.55
1.43
1.31
1.19
1.07
0.94
0.82
0.70
Chemical shift

Figure 2

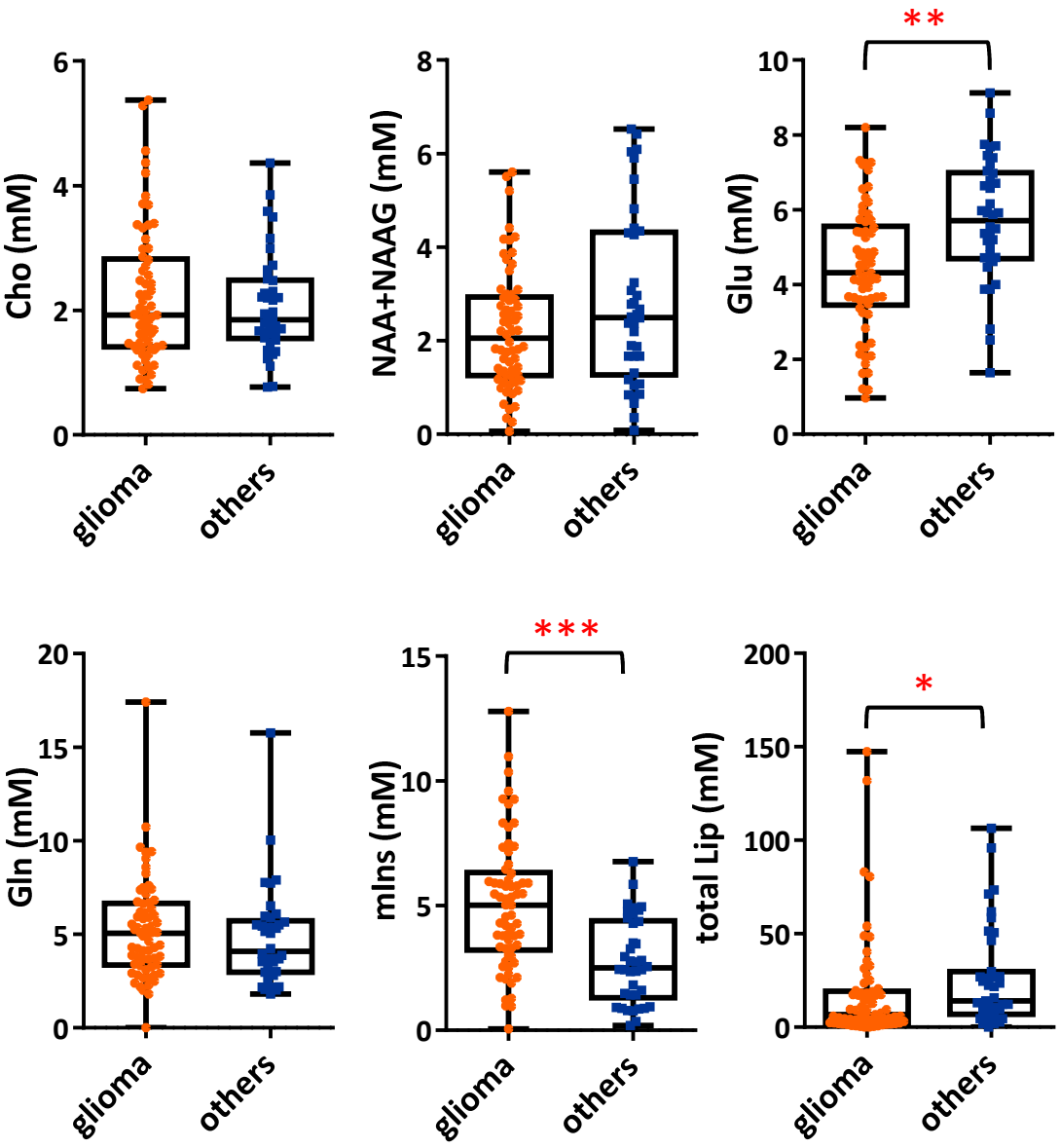
Cho (mM)
NAA+NAAG (mM)
Glu (mM)
Gln (mM)
mIns (mM)
total Lip (mM)
glioma
others
**
***
*

Figure 3

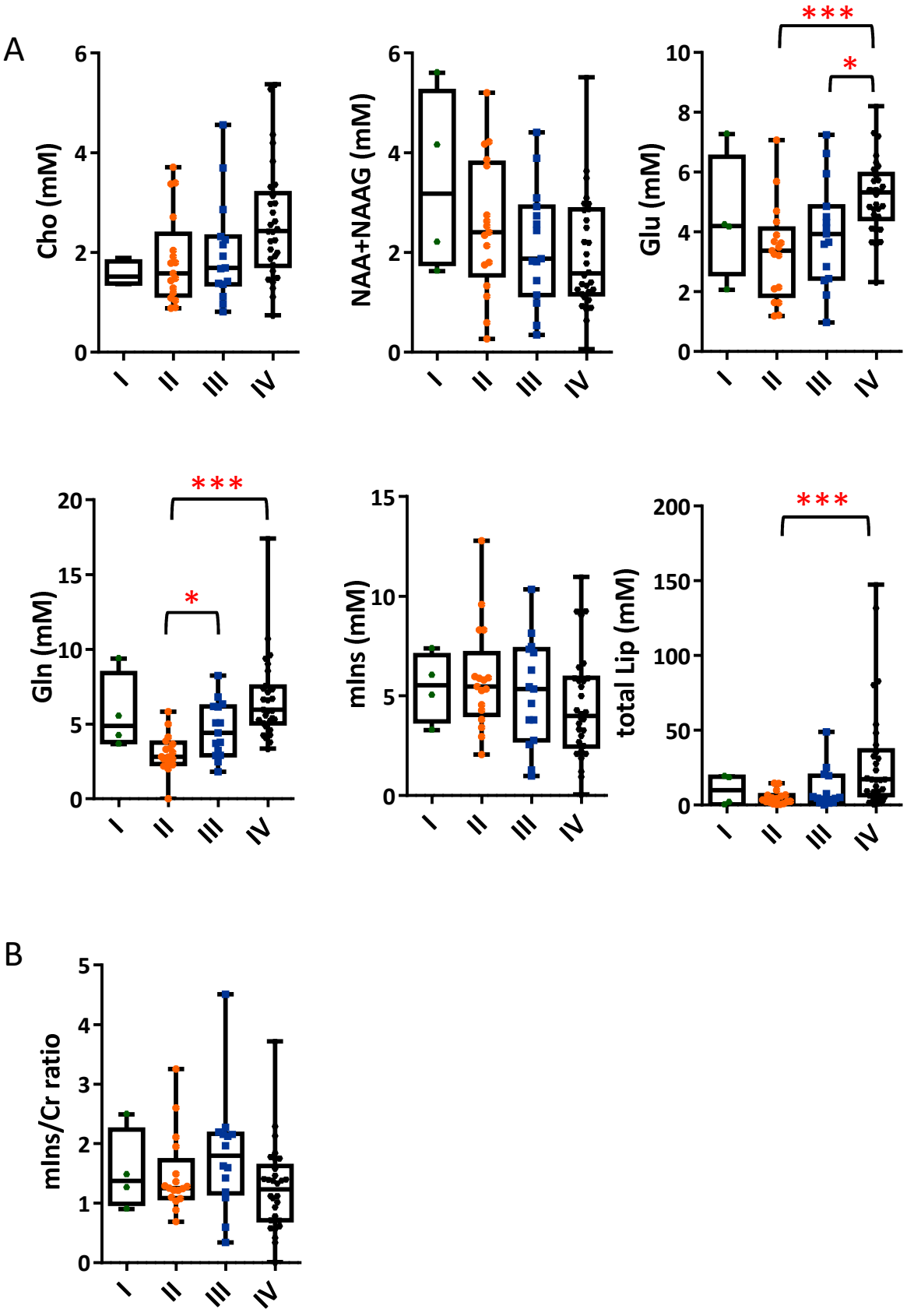
A
Cho (mM)
NAA+NAAG (mM)
Glu (mM)
Gln (mM)
mIns (mM)
total Lip (mM)
B
mIns/Cr ratio
I
II
III
IV
*
***

Supple Figure 1

A

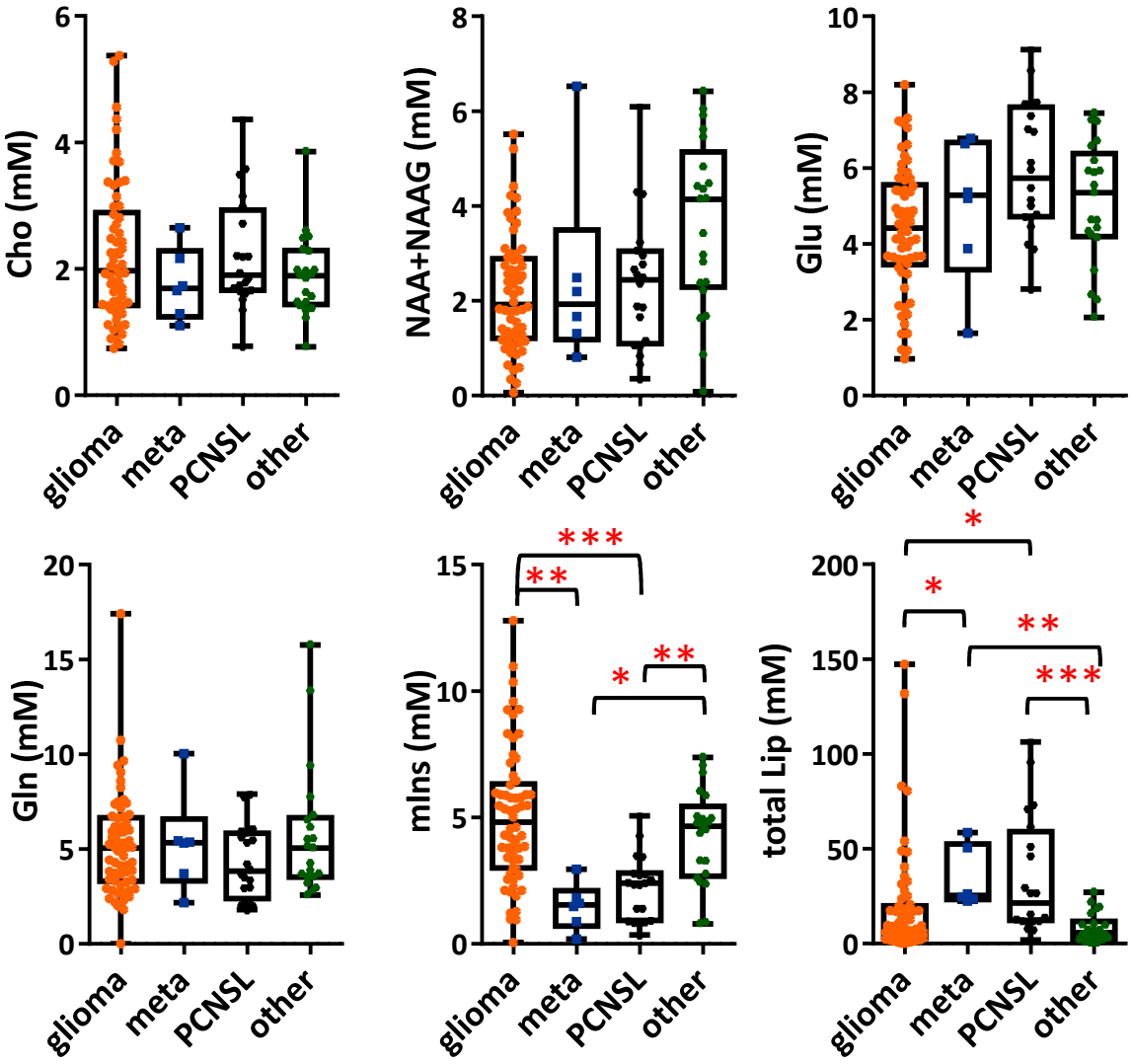

B

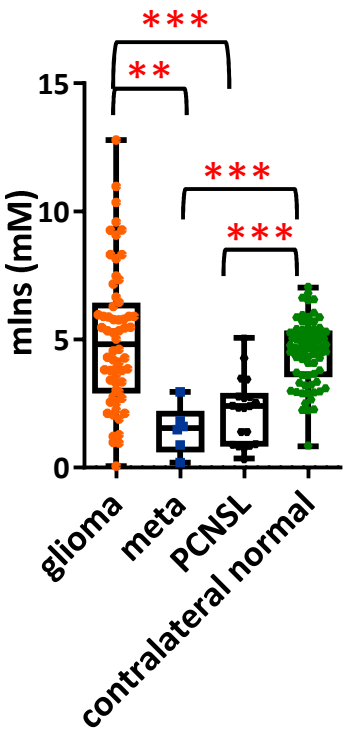

Supple Figure 2

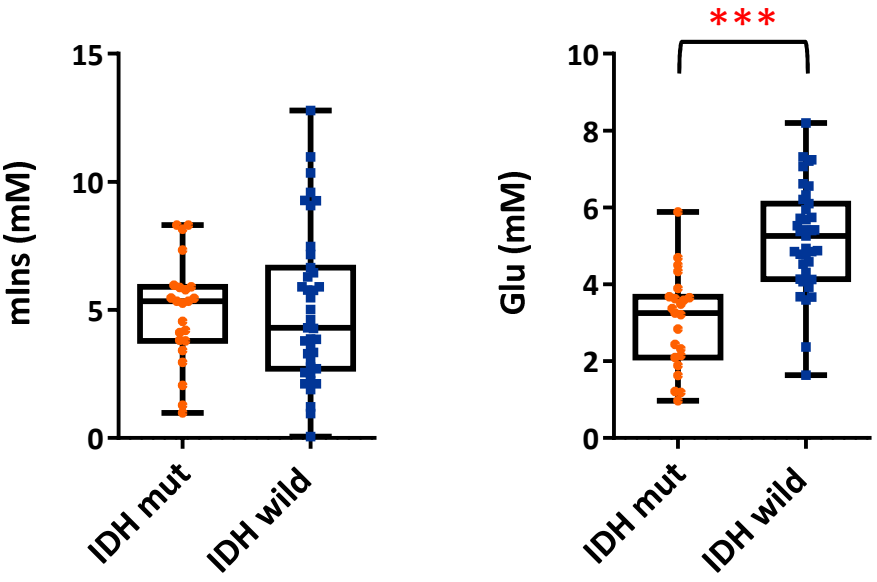

Supple Figure 3

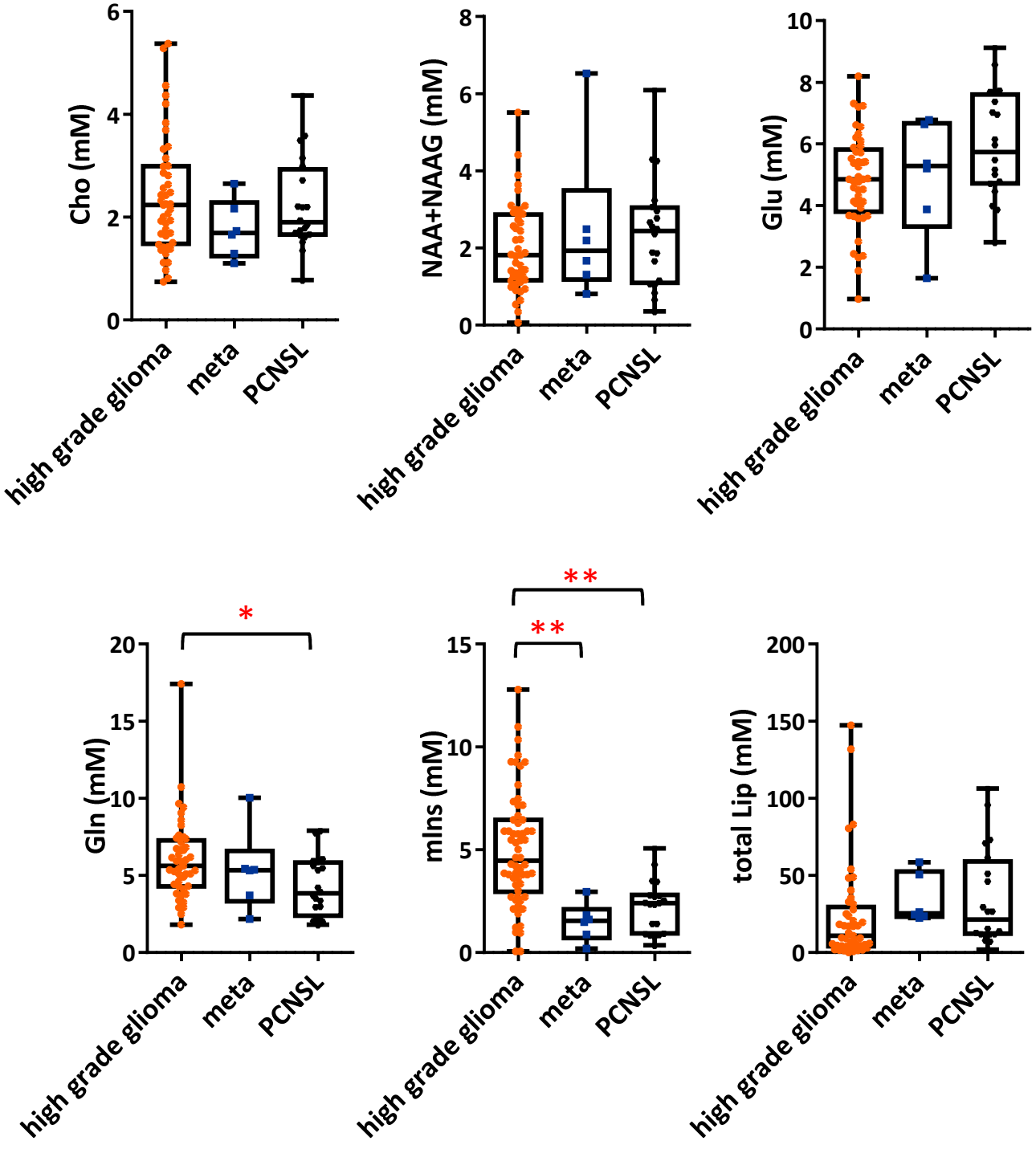

Supple Figure 4

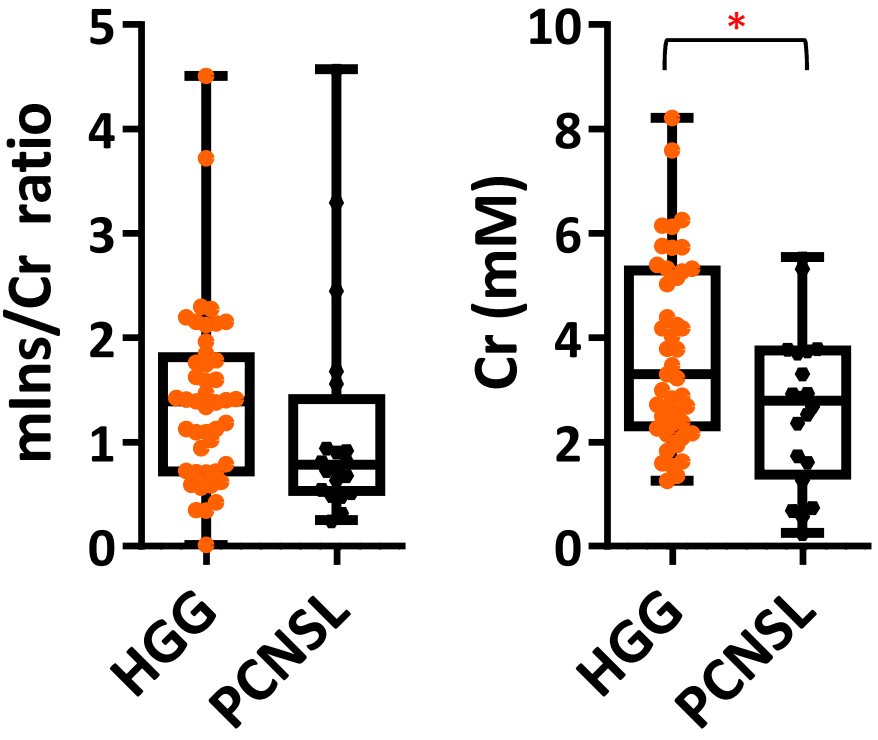

Supple Figure 5

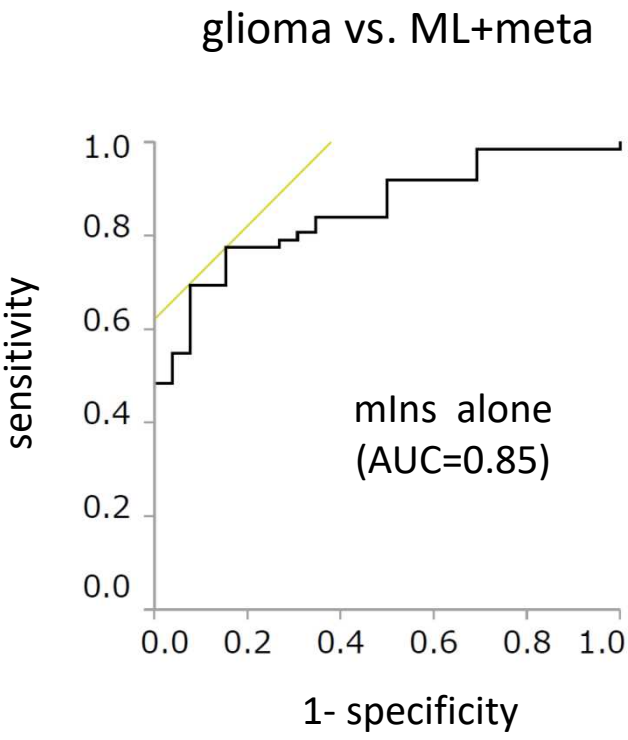

Supple Figure 6